Femtosecond transient absorption spectroscopy of silanized silicon quantum dots

Volker Kuntermann, Carla Cimpean, Georg Brehm, Guido Sauer, and Carola Kryschi*
Department of Physical Chemistry I and the Interdisciplinary Center for Molecular Materials, Friedrich-Alexander University of Erlangen-Nuremberg, Egerlandstrasse 3, D-91058 Erlangen, Germany

Hartmut Wiggers
Institute for Combustion and Gas Dynamics, University of Duisburg-Essen, Lotharstrasse 1, D-47048 Duisburg, Germany
(Received 18 May 2007; revised manuscript received 28 September 2007; published 24 March 2008)

Excitonic properties of colloidal silicon quantum dots (Si qdots) with mean sizes of 4 nm were examined using stationary and time-resolved optical spectroscopy. Chemically stable silicon oxide shells were prepared by controlled surface oxidation and silanization of HF-etched Si qdots. The ultrafast relaxation dynamics of photogenerated excitons in Si qdot colloids were studied on the picosecond time scale from 0.3 ps to 2.3 ns using femtosecond-resolved transient absorption spectroscopy. The time evolution of the transient absorption spectra of the Si qdots excited with a 150 fs pump pulse at 390 nm was observed to consist of decays of various absorption transitions of photoexcited electrons in the conduction band which overlap with both the photoluminescence and the photobleaching of the valence band population density. Gaussian deconvolution of the spectroscopic data allowed for disentangling various carrier relaxation processes involving electron-phonon and phonon-phonon scatterings or arising from surface-state trapping. The initial energy and momentum relaxation of hot carriers was observed to take place via scattering by optical phonons within 0.6 ps. Exciton capturing by surface states forming shallow traps in the amorphous SiO_x shell was found to occur with a time constant of 4 ps, whereas deeper traps presumably localized in the Si-SiO_x interface gave rise to exciton trapping processes with time constants of 110 and 180 ps. Electron transfer from initially populated, higher-lying surface states to the conduction band of Si qdots (>2 nm) was observed to take place within 400 or 700 fs.

DOI: 10.1103/PhysRevB.77.115343 PACS number(s): 73.22.−f

I. INTRODUCTION

Silicon (Si) nanostructures have stimulated intense research activities because of their potential applications to electronic devices and microphotonics.[1–3] Charge carrier motions in nanoelectronics devices operate at length scales of electron mean free paths ranging between 5 and 10 nm in bulk silicon at room temperature. The corresponding transit times are picoseconds and less. This time scale is the domain of electron and phonon scatterings and that of trapping by surface states which are localized, for instance, in the native passivation layer of Si. Hence, successful development of high-speed nanoelectronics devices such as single-hole transistors[4] requires comprehensive investigations of the relaxation dynamics of charge carriers (i.e., electrons and holes) in nanoscale Si on an ultrashort time scale down to femtoseconds. This may be achieved by examining the initial decay dynamics of photogenerated excitons which occur via elastic and inelastic carrier-carrier scatterings and carrier-phonon scattering.[5]

Bulk Si crystallizes in a cubic diamond lattice and is an indirect band gap semiconductor. This implies for its optical properties that the direct $\Gamma \rightarrow \Gamma$ transition (at $\mathbf{k}=0$) reaches a saddle point of the conduction band, whereas the lowest energetic $\Gamma \rightarrow X$ transition violates the law of momentum conservation and requires therefore the assistance of transversal optical (TO) or transversal acoustic (TA) phonons.[5] For Si quantum dots (qdots) having sizes smaller than the exciton Bohr diameter of 8.6 nm,[6] the laws of momentum conservation are relaxed.[7] The motions of carriers and phonons are confined in all three spatial dimensions, and their wave functions are spread out in the $\mathbf{k}$ space. Direct consequences of the quantum confinement effect are a modified energy band structure, altered electron-phonon couplings, and enhanced transition probabilities of the optical zero-phonon and phonon-assisted transitions.[5,7,8] In particular, quantum confinement leads to large amplitudes of the carrier wave functions at the surface. The resulting efficient carrier interactions with surface states facilitate indirect-band-gap transitions by scattering as well as they may induce ultrafast exciton trapping and recombination.[7,9–11]

Stationary and time-resolved spectroscopy of Wannier-Mott excitons in Si nanostructures has been in the focus of extensive experimental and theoretical activities in recent past.[8–22] Si qdots in porous Si (Ref. 12) and Si qdots grown by annealing Si-ion-implanted SiO_2 films[13,14] or prepared by electrochemical etching of Si wafers[1] were observed to exhibit two species of photoluminescence (PL). The size-independent blue PL was ascribed to radiative recombination of trapped excitons which are localized at defects in the Si-SiO_x interface[15] or at oxygen vacancies in the amorphous SiO_x shell.[16,17] The other PL species depends on the size of the Si qdots and is therefore attributed to the radiative recombination of quantum-confined excitons.[21] The corresponding $X \rightarrow \Gamma$ transition was observed to be predominantly assisted by the momentum conserving TO phonon at 57.3 meV or the TA phonon at 19 meV,[22] while the zero-phonon transition is predicted to become probable because of the relaxed momentum conservation rule. The lifetime of the quantum-confined exciton PL was reported to depend on the detection energy and to range between 1 and 60 μs.[17,23,24] The rather long lifetimes do not allow for direct monitoring

the temporal evolution of the PL spectra using luminescence up-conversion techniques.

Essential information of ultrafast carrier dynamics in Si qdots can be achieved by femtosecond resolved pump-probe spectroscopy which is sensitive to both the absorption of photogenerated electrons in the conduction band and the bleaching by the correspondingly diminished population density in the valence band.[5,25] In this spectroscopy technique, an ultrashort laser pump pulse generates quantum confined excitons in Si qdots via absorption transitions of valence-band electrons to the conduction band. Excitation with photon energies larger than the band gap creates hot carriers as being electrons and holes with excess kinetic energies and specific momenta. Intraband relaxation dynamics of hot carriers may take place by dephasing and thermalization within the conduction or the valence band. Dephasing occurs via momentum-relaxing carrier-carrier scattering in a few hundred femtoseconds,[26] while scattering of hot carriers by longitudinal-optical (LO) phonons [E_{LO}=53 meV (Ref. 27)] causes a thermalization with the lattice on a time scale between a few hundred femtoseconds and several picoseconds.[28] Complete relaxation of the electrons to one of the six degenerate (100)-valleys of the conduction band[29] requires the dissipation of the excess kinetic energy via sequential emission of smaller-energy acoustic phonons on a time scale up to hundreds of picoseconds.[5] The multiphonon processes may be induced by lattice anharmonicities or by surface states. They become progressively slower with decreasing energy until a phonon bottleneck is reached.[3] A competing process is trapping of photoexcited carriers by surface states which also may occur on the early picoseconds time scale.[11]

Up to now, only Klimov *et al.*[25] have applied femtosecond transient absorption spectroscopy for the study of photogenerated carrier dynamics in Si qdots. Their samples consisted of Si qdots embedded in amorphous SiO_2 films. They observed initial carrier decay dynamics on the sub-10 ps time scale which they assigned to efficient surface-state trapping. Although intense theoretical and experimental research activities have been devoted to the elucidation of photophysical properties of Si qdots, the ultrashort relaxation dynamics of excitons are hardly understood until now. In particular, the contribution of surface states to dephasing and thermalization of hot carriers is a long-standing issue of the physics of semiconductor qdots.[19] The reason for this is the native passivation layer of Si nanostructures. The nonstoichiometric composition and amorphous structure of the SiO_x shell critically depend on the preparation technique and environmental conditions and may significantly alter by aging. This implies that the structural and electronic properties of surface states are difficult to control or to be reproducibly prepared.

In this paper, we present a femtosecond spectroscopy study of ultrashort exciton relaxation dynamics in silanized Si qdots with mean sizes of 4 nm. Si qdots with natively oxidized surfaces were prepared via rf-induced decomposition of silane. Stabilized surface structures were obtained by the removal of the native passivation layer by HF etching followed by reoxidization under controlled conditions. Stabilization of the SiO_x shell was achieved by silanization. The silanized Si qdots were dispersed in cyclohexane. Irradiation of the Si qdots dispersion with 150 fs pump pulses at 390 nm generated quantum-confined excitons via one photon absorption transitions of valence band electrons.[23] The temporal evolution of the absorption and bleaching of photogenerated carriers were probed between 0 and 2.3 ns using variably delayed 150 fs pulses of a white-light continuum. The analysis of the transients allowed us to discriminate between distinct decay dynamics of the excitons. The short time behavior ($<$5 ps) was assigned to electron-LO-phonon scattering and exciton trapping by surface states, which form shallow traps. Couplings of the photoexcited electrons with large wave vector phonons (TA or LA phonons) providing complete intraband relaxation or capture of the photoexcited electrons by deep traps localized at the Si-SiO_x interface were discussed to be responsible for the observed long time behavior ($>$100 ps).

II. EXPERIMENT

A. Materials

Si qdots with a mean size of 4 nm were prepared in a low-pressure rf reactor using silane as a precursor.[30] Trichlorododecylsilane (Aldrich, purum, $\geqslant$95.0%), cyclohexane (Fluka, $\geqslant$99.5%), 2-propanol (Fluka, $\geqslant$99.5%), and aqueous hydrofluoric acid (Riedel-de Han, $\geqslant$40%) were used as received.

B. Surface treatment

All wet-chemistry procedures were performed under ambient conditions. 40 ml of 1:1 mixture of cyclohexane and 2-propanol were used to disperse 100 mg of Si qdots. The suspension was sonicated for 30 min. To remove the native passivation layer of the Si qdots by HF etching 20 ml of aqueous hydrofluoric acid (40%) were added and the suspension was stirred overnight. Two phases were formed: the lower polar phase consisted of 2-propanol, HF, and water, whereas the upper cyclohexane phase contained the etched Si qdots. 3 ml of trichlorododecylsilane were added to the yellowish suspension and the silanization was carried out by stirring the mixture at 2 °C for 2 h. Finally, the silanized Si qdots were washed several times with cyclohexane using an ultracentrifuge (Heraeus, sepatech).

C. Steady-state spectroscopy

The photoluminescence spectra were recorded on a Jobin-Yvon FluoroMax-3 spectro-fluorometer using the magic-angle polarization configuration. All experiments were performed at room temperature employing quartz cuvettes with a thickness of 10 mm. Silanized Si qdots were dispersed in cyclohexane at a concentration of 100 μg/ml.

D. Time-resolved spectroscopy

Femtosecond transient absorption spectroscopy experiments were conducted with a Clark MXR CPA 2001 laser system in conjunction with an Ultrafast Systems detection system, consisting primarily of a glass fiber based spectrometer. The output pulses (at 390 nm) of this laser system, used

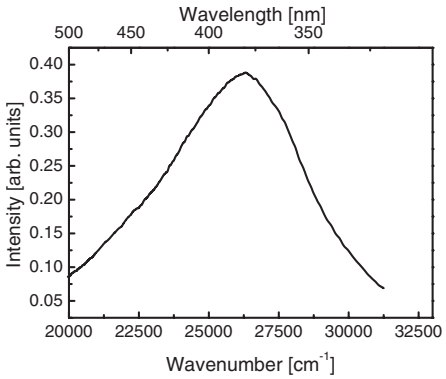

FIG. 1. PL spectrum of silanized Si qdots: the surface-state PL was excited at 300 nm.

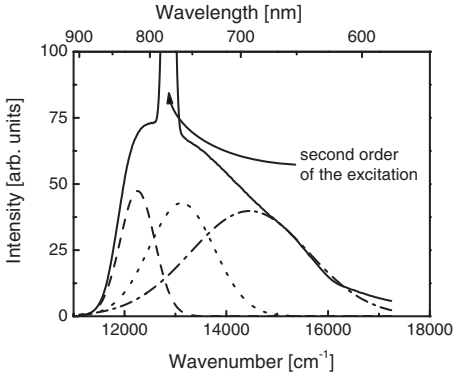

FIG. 2. PL spectrum of silanized Si qdots: the exciton PL was excited at 390 nm (black solid line); the PL intensity distribution is simulated by a superposition of three Gaussians (dashed, dotted, and dashed-dotted black lines).

as pump pulses, are amplified frequency-doubled pulses of the Er^{3+} doped glass fiber oscillator. Their pulse duration is about 150 fs [full width at half maximum (FWHM)] and their repetition rate is 1 kHz. All samples were pumped at excitation densities between 1.14×10^9 and 1.90×10^9 W/cm^2. The samples consisting of 2 mg Si qdots dispersed in 1 ml cyclohexane were irradiated in quartz cuvettes with a thickness of 2 mm. A fraction of the fundamental was simultaneously passed through a sapphire plate to generate a femtosecond white-light continuum between 400 and 1200 nm. The chirp between 400 and 750 nm was approximately 350 fs. Transient absorption spectra of silanized Si qdots in cyclohexane were taken at delay times between −2 ps and 2.3 ns. They were recorded in the visible between 400 and 750 nm or in the near infrared (NIR) between 800 and 1200 nm. No photochemical degradation was observed after each experiment as subsequent detecting of the sample by luminescence spectroscopy has revealed.

PL decay profiles were recorded using the time-correlated single-photon counting (TCSPC) luminescence technique. PL of a Si qdot cyclohexane dispersion in a 10 mm quartz cuvette was excited using the 390 nm output pulses of the Clark MXR CPA 2001 laser system, while the time-resolved measurement of the PL intensity was carried out on the TCSPC spectrometer Fluorolog-3 (Jobin Yvon) equipped with a microchannel plate (Hamamatsu, R3809U-50) that provides a time resolution of about 60 ps.

III. RESULTS AND DISCUSSION

PL of passivated Si qdots may originate either from localized surface states of the amorphous SiO_x shell or from quasidelocalized states of quantum confined excitons.[8–22] Figures 1 and 2 show the PL spectra of silanized Si qdots dispersed in cyclohexane. The blue PL peaking at 380 nm was excited at 300 nm (Fig. 1) and is ascribed to a distribution of energetically distinct surface states of the amorphous SiO_x shell. Irradiation of the Si qdot sample with 390 nm light produced the red PL at 800 nm (Fig. 2) which was attributed to radiative electron-hole recombinations between quantized states near the minimum of the conduction band and those at the valence band maximum. The weakly structured and asymmetric PL intensity distribution essentially resembles the PL spectrum of similarly prepared Si qdots with a mean diameter of 4.1 nm.[23] For ideally spherically shaped Si qdots, the non-Gaussian intensity distribution of the PL spectrum as being composed of at least three Gaussians (see Fig. 2: dotted, dashed, and dashed-dotted lines) may be explained with distinctly weighted Gaussian size distributions, giving rise to each other overlapping PL bands. Since the HF-etching procedure will considerably alter the initially spherical shapes of the Si qdots, the PL intensity distribution does not any more depend via the radiative transition probability on one Gaussian size distribution.[31] An ensemble of Si qdots with different shapes and sizes cannot be rationalized by any standard distribution function. The PL excitation (PLE) spectrum detected at 750 nm (see Fig. 3) consists of a broad band with a prominent maximum at 340 nm (29 411 cm^{-1}) and a shoulder at 390 nm (25 640 cm^{-1}). The large Stokes shift of about 16 100 cm^{-1} is consistent with the indirect-band-gap structure that is obviously still retained in 4 nm sized Si qdots. On the other hand, its FWHM of about 12 000 cm^{-1} need not only arise from the wide size distribution of the Si qdots but may also partially stem from the relaxed law of momentum conservation. In addition to indirect phonon-assisted transitions, the direct zero-phonon transition becomes more probable due to the spread of the electron wave functions in the **k** space.

The decay dynamics of quantum-confined excitons generated with 150 fs pump pulses at 390 nm were monitored

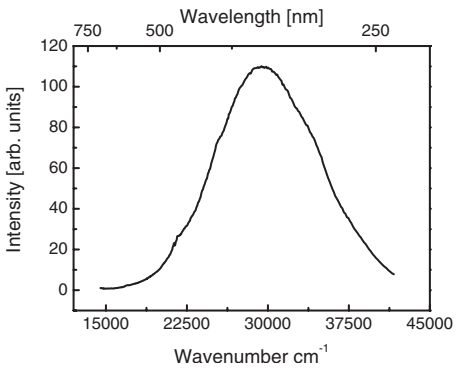

FIG. 3. PLE spectrum of the exciton PL detected at 750 nm.

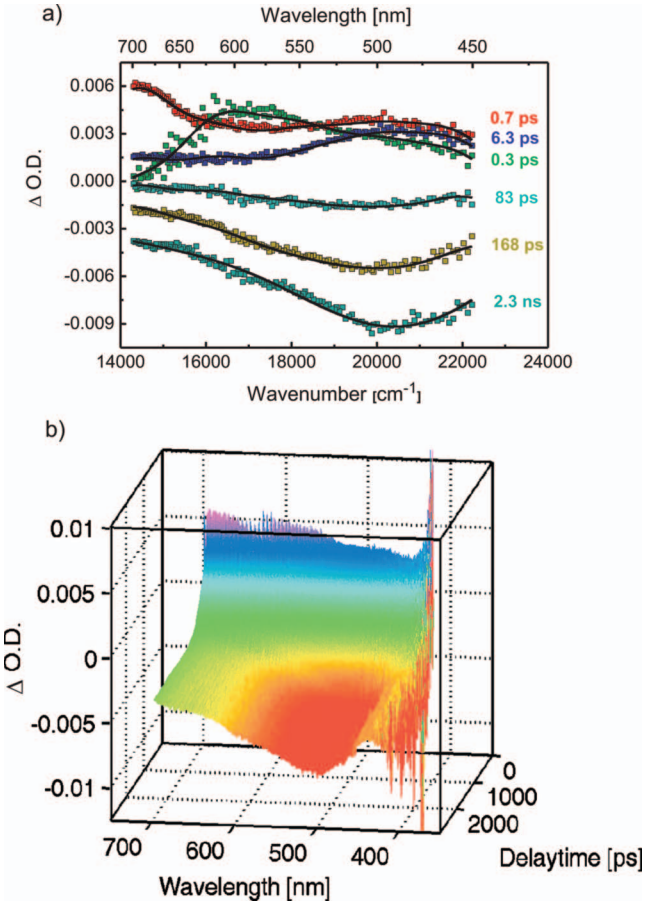

FIG. 4. (Color) (a) Temporal evolution of the transient absorption spectra (squares: experimental data and line: simulation) in the visible for distinct delay times between 0.3 ps and 2.3 ns. (b) Temporal evolution of the transient absorption spectra in the visible for distinct delay times between 0 ps and 2.3 ns in a 3D representation.

using a temporally delayed femtosecond white-light continuum pulses. The pump pulse induced changes in the absorption of the Si qdots were recorded in the visible (400–750 nm) and in the NIR (800–1200 nm). The peak power of the pump pulse was varied between 1.14×10^9 and 1.90×10^9 W/cm^2, where no noticeable difference in spectral features and decay traces of the transient absorption spectra could be observed. Figures 4(a) and 4(b) depict the temporal evolution of the transient absorption spectra recorded in the visible as (a) two-dimensional and (b) three-dimensional (3D) plots.

The transient absorption spectrum at 0.3 ps after excitation exhibits a prominent photon-induced absorption (PA) band (ΔOD>0) (OD denotes optical density) at 600 nm [see Fig. 4(a)]. With rising the delay time to 0.7 ps, the initial PA band decreases with the emerge of two new PA bands at 470 and 700 nm that decay on a time scale of a few hundreds of picoseconds. At a delay time of 2.3 ns, photoinduced absorption completely vanishes, while a photon-induced bleaching (PB) spectrum (ΔOD<0) is left over. The complex spectral features of the transient absorption spectra obviously originates from a superposition of photobleaching with at least three photoinduced absorption transitions. In order to analyze the time evolution of the involved spectral components, we have decomposed the transient absorption spectra of a representative selection into, respectively, eight Gaussian functions with fix peak positions and widths, whereas their amplitudes were varied with the delay time until the best fit was obtained [see line plot in Fig. 4(a)]. The PA bands at 470, 600, and 700 nm were accounted for by a sum of three Gaussians (19 800, 21 500, and 22 300 cm^{-1}), a sum of two Gaussians (16 200, and 17 800 cm^{-1}) and one Gaussian (14 300 cm^{-1}), respectively. Since the photogeneration of electron-hole pairs will have taken place within the temporal pump-pulse width (150 fs) and the recovery of the valence-band population density requires both radiative and nonradiative recombinations of the excitons that occur in the microsecond regime,[23,24] the bleaching spectrum is assumed to be instantaneously formed and to remain constant on our time scale of study. The bleaching spectrum at 2.3 ns was simulated by a sum of two Gaussians at 15 000 and 20 800 cm^{-1} with negative amplitudes. The transient absorption spectra depicted in Fig. 4(a) were simulated by the sum of the eight Gaussians by varying the amplitudes of those describing the PA bands and by keeping constant the amplitudes of the PB spectrum, the peak positions, and widths of all Gaussian functions. Figure 5(a) represents two transients detected 550 and 600 nm which characterize the ultrafast decay behavior of the PA band at 600 nm. Hence the measured decay curves $\Delta\mathrm{OD}(t)$ are approximated by a convolution of the apparatus response function $G(t)$ with a biexponential decay function $f(t)$: $\Delta\mathrm{OD}(t)\propto f(t)\otimes G(t)$, with $f(t)=a\exp(-t/\tau_{\text{el-ph}})+b\exp(-t/\tau_{\text{trap}})$. The apparatus response function $G(t)$ was obtained as a Gaussian function with a width of 210 fs, whereas the biexponential decay curves were consistently fitted with the time constants of 0.57 and 4 ps. Since dephasing by electron-electron scattering under ambient conditions presumably occurs within a few tens of femtoseconds,[32] the shortest time constant, $\tau_{\text{el-ph}}=0.57$ ps, is ascribed to electron-LO-phonon scattering. Subsequent phonon scattering processes contributing to the electron relaxation to the conduction band minimum should involve the emission of lower-energy acoustic phonons and thus was predicted to occur on a time scale of hundreds of picoseconds and more. The competitive decay process is assigned to trapping of the photoexcited electrons with the time constant $\tau_{\text{trap}}=4$ ps. Shallow surface states formed by surface-standing Si=O bonds are argued to act as suitable traps.[10] The assignment of the short-time behavior to trapping events is consistent with the results reported by Klimov *et al.*[25] which were obtained from a femtoseconds transient absorption spectroscopy study of Si qdots in SiO_2 films.

The rise of the PA bands at 470 and 700 nm and the long-time decay profiles of all three PA bands were examined by analyzing the temporal evolutions of the respective amplitudes of the Gaussian functions used for the simulation of the transient absorption spectra [Fig. 4(a)]. For the PA band at 700 nm, one Gaussian amplitude scales with the ΔOD of the band, while in the case of the PA bands at 600 and 470 nm, the respective arithmetic mean value of the amplitudes were taken as a relative measure for the ΔOD. Figure 5(b) shows the time behavior of the amplitudes and of their mean values which display the temporal evolution of the PA

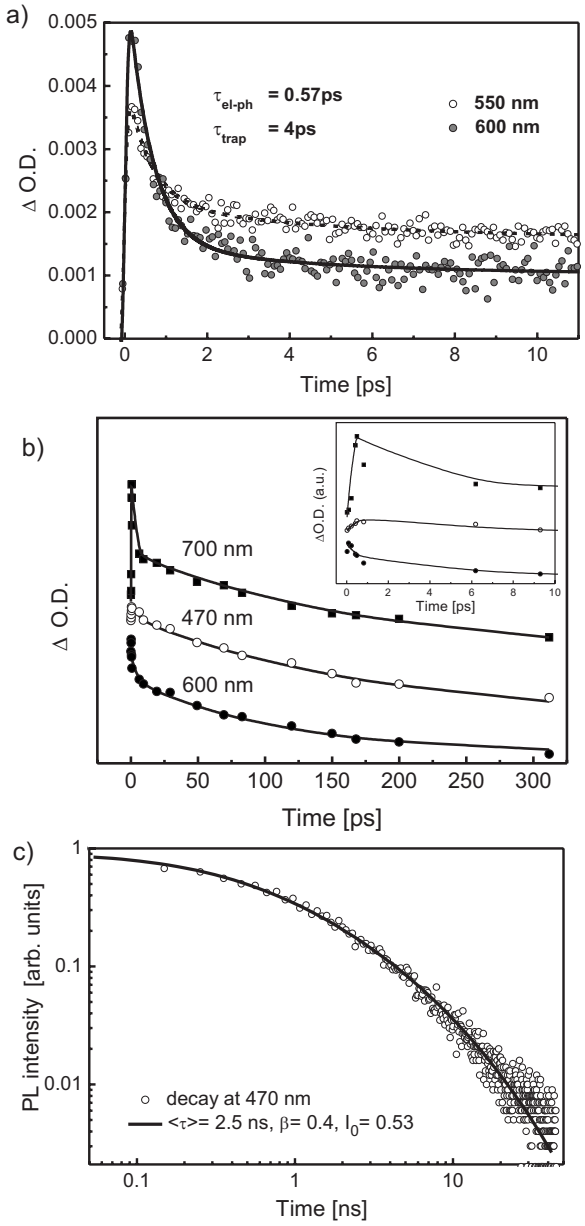

FIG. 5. (a) Short-time behavior of the PA transients detected at 550 and 600 nm. The temporal evolutions of the Gaussian amplitudes simulating rise and decay dynamics of the PA bands at 470 nm (open circles), 600 nm (solid circles), and at 700 nm (solid squares) depicted in (b) were fitted for the 600 nm data with a triexponential decay function and for the 470 and 700 nm data with a superposition of an exponential rise function and a triexponential decay function (solid line); their short-time behavior is presented in the inset. (c) shows the double logarithmic representation of the experimental PL decay profile (open circles) and the stretched exponential fit function (solid line) with the fit parameters given in the legend.

bands at 470 nm (open circles), 600 nm (solid circles), and 700 nm (solid squares). While the PA band at 600 nm was instantaneously formed, the PA bands at 470 and 700 nm were observed to emerge within 700 and 400 fs, respectively. The decay dynamics of all PA bands are nonexponential and obviously contain short-time and long-time components. The obvious resemblances in their decay traces suggest to assume that at first, the observed PA transitions occur from different **k** states of the conduction band and that, second, their initial decay processes are similarly dominated by electron LO-phonon scattering and fast trapping of the photoexcited electrons in shallow traps. Thus, the decay dynamics of the 600 nm PA band is fitted by a three-exponential function containing as three independent relaxation processes the electron-LO-phonon scattering with the time constant $\tau_{\text{el-ph}}=0.57$ ps, the electron trapping with $\tau_{\text{trap}}=4$ ps and a slower relaxation process with $\tau_{\text{slow1}}=110$ ps. The latter relaxation channel might be either caused by the interaction of the conduction band electrons with large wave vector phonons (i.e., LA or TA phonons) associated with lattice anharmonicity or surface states[33] or arise from the capture of the electrons by deep traps localized in the interface between the Si core and the SiO_x shell. The ultrafast rise dynamics of the PA bands at 470 and 700 nm [see inset of Fig. 5(b)] are ascribed to electron transfer from initially populated, higher-energy surface states of the SiO_x shell to momentum states of the conduction band which are sufficiently far from the center of the Brilloiun zone to give rise to the redshifted and blueshifted PA transitions at 700 and 470 nm. According to the three-zone model developed by Wolkin *et al.*[34] surface states due to Si═O bonds in the SiO_x shell of Si qdots with sizes larger than 2 nm lie above the conduction band and were presumably excited with the 390 nm pump pulse by photon absorption. The short-time decay behavior of the 470 and 700 nm PA bands resembles that of the PA band at 600 nm, whereas their slow decay component exhibits a significantly longer time constant with $\tau_{\text{slow2}}=180$ ps [see Fig. 5(b)]. The difference in τ_{slow1} and τ_{slow2} corroborates the assignment of the underlying decay process to conduction band-electron capture by deep traps which may considerably differ in their energies for Si qdots with sizes smaller than 2 nm compared to those larger than 2 nm. The surface-states PL decay dynamics were examined in the 0–50 ns region under the excitation conditions of the femtosecond transient absorption spectroscopy experiment using the TCSPC technique. Si qdots dispersed in cyclohexane were excited with the 150 fs pump pulse at 390 nm, while the PL decay profile at 470 nm was recorded on the TCSPC Fluorolog-3 spectrometer. As the structural disorder and nonstoichiometric composition of the SiO_x shell suggest, the PL decay profile [see Fig. 5(c)] is clearly nonexponential and obviously consists of a distribution of slightly different components on the nanoseconds scale. Differences in the local environment of the surface states lead to variations in the relaxation time and thereupon to a distribution of relaxation times which is properly modeled by the stretched exponential function[6] $I(t)=I_0(t)(\tau/t)^{1-\beta}\exp-(t/\tau)$. Here, τ is the effective PL lifetime, β is the dispersion factor ranging between 0 and 1, and I_0 is the amplitude. The solid line in Fig. 5(c) through the experimental data (open circles) is obtained as least square fit with the stretched exponential yielding the parameters $I_0=0.53$, $\tau=2.5$ ns, and $\beta=0.4$. The relatively small value of β reflects large structural disorder in the amorphous SiO_x shell and thereby the spread of the surface-state energies. On the other hand, the rather short effective lifetime $\tau=2.5$ ns inevitably associated with a high radiative transition probability mani-

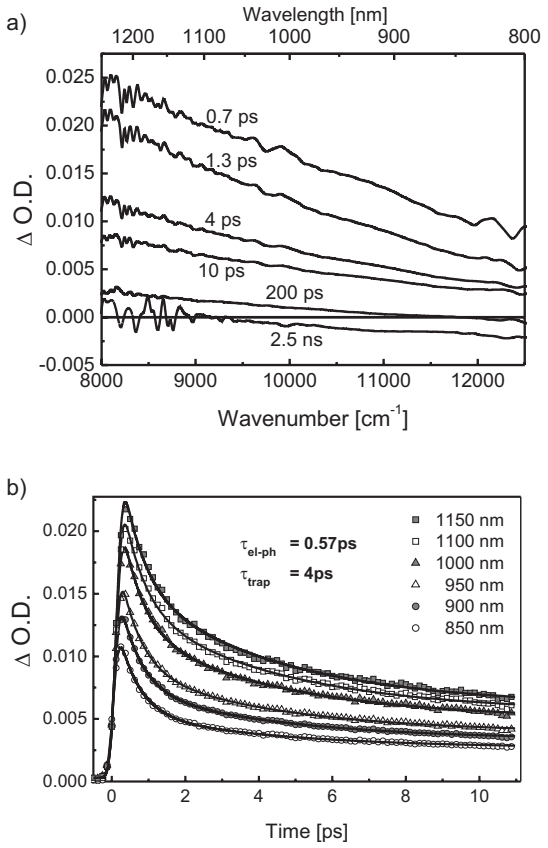

FIG. 6. (a) Temporal evolution of the transient absorption spectra in the NIR for distinct delay times between 0.7 ps and 2.5 ns. (b) Short-time behavior of the transients detected at wavelength between 850 and 1150 nm and fitted to a biexponential function with the time constants $\tau_{\text{el-ph}}$ and τ_{trap}.

fests the localized nature of the surface states. Despite the fact that the 390 nm pump pulse may provide either indirect population of the surface states via photogeneration of excitons in the Si core and subsequent trapping by lower energy surface states (for Si qdot sizes <2 nm) or direct excitation of the surface states (for Si qdot sizes >2 nm), no surface-state PL with decay dynamics around 2.5 ns were observed in any femtoseconds transient absorption spectroscopy experiment. Fig. 6(a) displays the time evolution of the transient absorption spectra which were recorded in the NIR. In contrast to those measured in the visible [see Figs. 4(a) and 4(b)], there are no pronounced structures, but a smooth rise in photoinduced absorption from 800 to 1200 nm. This observation is consistent with the IR absorption of free electrons in *n*-doped Si which was ascribed to transitions of electrons from the conduction band minima to a higher-lying energy band.[35] Free electrons in *n*-doped Si presumably correspond to the photogenerated electrons in Si qdots when they were completely thermalized and have relaxed to the conduction band minima. At delay times above 1 ns, spectral features with negative ΔOD values have been formed which were ascribed to the exciton PL (see Fig. 3). There is no spectroscopic evidence for $\Gamma \rightarrow X$ absorption. This implies that the indirect-band-gap transition is very unlikely, thus rendering impossible the observation of the photoinduced bleaching in the NIR.

TABLE I. Parameters obtained from the merged deconvolution-biexponential fitting procedure; *a* and *b* are the amplitudes and $\tau_{\text{el-ph}}$ and τ_{trap} are the respective time constants.

	a	*b*	$\tau_{\text{el-ph}}$ (ps)	τ_{trap} (ps)
850 nm	0.59	0.22	0.57	4.0
900 nm	0.55	0.26	0.57	4.0
950 nm	0.51	0.29	0.57	4.0
1000 nm	0.46	0.33	0.57	4.0
1100 nm	0.42	0.36	0.57	4.0
1150 nm	0.40	0.38	0.57	4.0
1200 nm	0.38	0.40	0.57	4.0

The significantly different spectral features of the NIR transient absorption spectra in comparison with those monitored in the visible [see Figs. 4(a) and 4(b)] are explained by the lack of photoinduced bleaching in the NIR as well as by the differences in the density of states. However, the short-time behavior of the transient spectra detected in the NIR agrees very well with that of those detected in the visible [see Fig. 6(a)]. The PA transients in the wavelength range between 850 and 1150 nm were analogously analyzed using the merged deconvolution-biexponential fitting procedure.

The values obtained for the respective two amplitudes, *a* and *b*, and two time constants, $\tau_{\text{el-ph}}$ and τ_{trap}, are summarized in Table I. While the values of $\tau_{\text{el-ph}}$ and τ_{trap} coincide with those of the transients detected in the visible, the two amplitudes reflect a clear dependency on the detection wavelength: with rising detection wavelength, the amplitude of the exponential function accounting for the trapping process increases at the expense of the decay process due to electron-LO-phonon scattering. This might be understood in context with the spread out of the electron wave functions in the **k** space that has been enlarged by initial electron-electron scattering. As an immediate consequence, the electrons distinctly smeared out in the **k** space may experience different probabilities for the electron-phonon scattering and trapping processes. The long-time decay behavior of the transients additionally involves the rise of the photoluminescence in the spectral range up to 1000 nm, whereas at longer detection wavelengths, the only contributing process is that from the decay of the photoinduced absorption. For the sake of comparison, the transients were fitted either by a monoexponential decay function for the PA or by a biexponential function accounting for the decay of PA and rise of PB. The decay and rise times are in in good agreement with the one obtained from fitting the transients in the visible.

IV. CONCLUSION

The PL spectrum of colloidal silanized Si qdots dispersed in cyclohexane consists of two emission bands, the maximum at 380 nm is assigned to surface states in the amorphous SiO_x shell of the Si qdots, while radiative recombination of the quantum confined excitons produces the PL band at 800 nm. Surface-state PL of Si qdots with sizes presum-

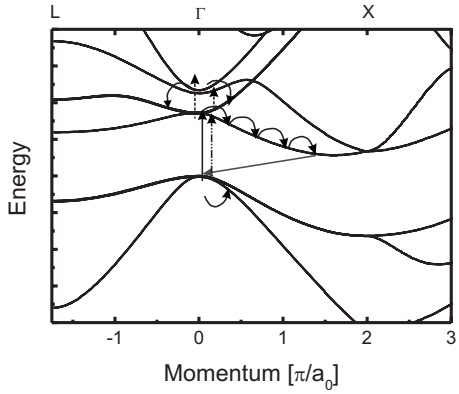

FIG. 7. Electronic band structure bulk Si: the excitons are created via an absorption transition (black arrow), the hot carriers relax to the valence band maximum and the conduction band minimum (curved black arrows), photoinduced absorption (dashed arrows) and bleaching (dashed-dotted arrow) take place around $\mathbf{k}=0$, whereas the exciton photoluminescence (gray arrow) occurs as a $X \rightarrow \Gamma$ transition.

ably larger than 2 nm was either directly excited by continuous uv light (<320 nm) or by 150 fs pump pulses at 390 nm. On the other hand, smaller-sized Si qdots are predicted to exhibit a band gap larger than the energy difference between the surface states[34] which may act as traps and radiative recombination centers for the quantum confined excitons. The exciton PL band at 800 nm is understood to originate from a non-Gaussian distribution of Si qdot sizes which includes sizes of about 1.5 nm and larger. The PLE spectrum peaking at 340 nm manifests the enlarged $\Gamma \rightarrow \Gamma$ band gap in comparison with bulk Si and its rather broad band width is probably due to the occurrence of zero-phonon and various phonon-assisted absorption transitions. For Si qdots with sizes larger than 3 nm, the ultrafast relaxation dynamics of hot carriers created by a 150 fs pump pulse at 390 nm can be described in terms of a simplified energy band structure scheme (see Fig. 7). Valence-band electrons are transferred via an absorption process (black arrows) into the conduction band of the Si qdot. Since there is an excess excitation energy, nonequilibrium electron and hole densities with specific momentum states and elevated temperatures are generated in the conduction band and valence band, respectively. As the system evolves temporally and spatially toward the thermal equilibrium with the lattice, momentum and energy relaxation will take place (curved black arrows). Elastic as well as inelastic carrier-carrier scattering processes randomize the momentum within tens of femtoseconds. The observed initial fast decay of photo-induced absorption with $\tau_{\text{el-ph}}=0.57$ ps is assigned to scattering of hot electrons by LO phonons. Scattering of the conduction band electrons at large wave vector phonons (i.e., LA or TA phonons) are discussed to be responsible for the significantly slower decays of the photoinduced absorption bands at 470, 600, and 700 nm that occurred with time constants of 110 and 180 ps. Subsequent thermalization may take place either via the decay of LO phonons into lower-energy phonons by multiphonon processes or by acoustic-phonon scattering of the conduction band electrons into one of the conduction band valleys. An alternative explanation for the slow decay dynamics employs the occurrence of deep traps in the interface which capture conduction-band electrons with a time constant different for Si qdots with sizes smaller and larger 2 nm. For Si qdots with sizes smaller than 1.5 nm, trapping by surface states dominates the exciton relaxation dynamics. The trapping process was ascribed to the exponential decay with $\tau_{\text{trap}}=4$ ps. The surface states of Si qdots with sizes between 1.5 and 3 nm were stated to act as traps for electrons only.[34] Consistently, the ultrafast rise dynamics of the PA bands at 470 and 700 nm are ascribed to electron transfer processes from initially photoexcited higher-lying surface states to the conduction band of Si qdots with sizes larger than 2 nm. Obviously, the size and shape distribution as well as the surface state energies may determine the contribution of trapping events to the ultrashort relaxation dynamics of the exciton and thereby the quantum yield of the exciton PL.

ACKNOWLEDGMENTS

Support of the Deutsche Forschungsgemeinschaft (Graduiertenkolleg 1161/1) is gratefully acknowledged. We are grateful to Christian von Borczyskowski for providing us with stimulating discussions on Si qdots. Furthermore, we thank L. Ley and J. Ristein for indicating to IR absorption properties of free electrons. In particular, we are grateful for generous support by Evonik Creavis and for the fruitful cooperation with A. Ebbers.

*Author to whom correspondence should be addressed; kryschi@chemie.uni-erlangen.de

[1] L. T. Canham, Appl. Phys. Lett. **57**, 1046 (1990).
[2] F. Huisken, B. Kohn, and V. Paillard, Appl. Phys. Lett. **74**, 3776 (1999).
[3] M. C. Hersam, N. P. Guisinger, and J. W. Lyding, Nanotechnology **11**, 70 (2000).
[4] M. Saitoh and T. Hiramoto, Appl. Phys. Lett. **84**, 3172 (2004).
[5] A. J. Nozik, Annu. Rev. Phys. Chem. **52**, 193 (2001).
[6] Y. Kanemitsu, Phys. Rep. **263**, 1 (1995).
[7] M. S. Hybertsen, Phys. Rev. Lett. **72**, 1514 (1994).
[8] J. D. Holmes, K. J. Ziegler, R. C. Doty, L. E. Pell, K. P. Johnston, and B. A. Korgel, J. Am. Chem. Soc. **123**, 3743 (2001).
[9] L. Brus, Phys. Rev. B **53**, 4649 (1996).
[10] G. Allan, C. Delerue, and M. Lannoo, Phys. Rev. Lett. **76**, 2961 (1996).
[11] K. Kimura, J. Cluster Sci. **10**, 359 (1999).
[12] J. C. Vial, A. Bsiesy, F. Gaspard, R. Herino, M. Ligeon, F. Muller, R. Romestain, and R. M. Macfarlane, Phys. Rev. B **45**, 14171 (1992).
[13] L. Khomenkova, N. Korsunska, T. Torchynska, V. Yukhimchuk, B. Jumayev, A. Many, Y. Goldstein, E. Savir, and J. Jedrzejew-

ski, J. Phys.: Condens. Matter **14**, 13217 (2002).
[14] H. Z. Song and X. M. Bao, Phys. Rev. B **55**, 6988 (1997).
[15] Y. Kanemitsu, S. Okamoto, M. Otobe, and S. Oda, Phys. Rev. B **55**, R7375 (1997).
[16] P. Duong, P. Lavallard, A. Oliver, and T. Itoh, Phys. Status Solidi C **0**, 1271 (2003).
[17] I. N. Germanenko, S. T. Li, and M. S. El-Shall, J. Phys. Chem. B **105**, 59 (2001).
[18] A. Smith, Z. H. Yamani, N. Roberts, J. Turner, S. R. Habbal, S. Granick, and M. H. Nayfeh, Phys. Rev. B **72**, 205307 (2005).
[19] J. Martin, F. Cichos, and C. von Borczyskowski, J. Lumin. **108**, 347 (2004).
[20] Z. F. Li, M. T. Swihart, and E. Ruckenstein, Langmuir **20**, 1963 (2004).
[21] G. Ledoux, O. Guillois, D. Porterat, C. Reynaud, F. Huisken, B. Kohn, and V. Paillard, Phys. Rev. B **62**, 15942 (2000).
[22] P. D. J. Calcott, K. J. Nash, L. T. Canham, M. J. Kane, and D. Brumhead, J. Phys.: Condens. Matter **5**, L91 (1993).
[23] L. Van Dao, X. M. Wen, M. T. T. Do, P. Hannaford, E. C. Cho, Y. H. Cho, and Y. D. Huang, J. Appl. Phys. **97**, 13501 (2005).
[24] C. Meier, A. Gondorf, S. Luttjohann, A. Lorke, and H. Wiggers, J. Appl. Phys. **101**, 103112 (2007).
[25] V. I. Klimov, C. J. Schwarz, D. W. McBranch, and C. W. White, Appl. Phys. Lett. **73**, 2603 (1998).
[26] A. J. Sabbah and D. M. Riffe, Phys. Rev. B **66**, 165217 (2002).
[27] D. Kovalev, H. Heckler, G. Polisski, J. Diener, and F. Koch, Opt. Mater. (Amsterdam, Neth.) **17**, 35 (2001).
[28] M. Harb, R. Ernstorfer, T. Dartigalongue, C. T. Hebeisen, R. E. Jordan, and R. J. D. Miller, J. Phys. Chem. B **110**, 25308 (2006).
[29] G. Allan and C. Delerue, Phys. Rev. B **66**, 233303 (2002).
[30] J. Knipping, H. Wiggers, B. Rellinghaus, P. Roth, D. Konjhodzic, and C. Meier, J. Nanosci. Nanotechnol. **4**, 1039 (2004).
[31] P. F. Trwoga, A. J. Kenyon, and C. W. Pitt, J. Appl. Phys. **83**, 3789 (1998).
[32] J. R. Goldman and J. A. Prybyla, Phys. Rev. Lett. **72**, 1364 (1994).
[33] A. Othonos, J. Appl. Phys. **83**, 1789 (1998).
[34] M. V. Wolkin, J. Jorne, P. M. Fauchet, G. Allan, and C. Delerue, Phys. Rev. Lett. **82**, 197 (1999).
[35] W. Spitzer and H. Y. Fan, Phys. Rev. **108**, 268 (1957).